IEEE Access
Multidisciplinary | Rapid Review | Open Access Journal

Received 27 June 2024, accepted 24 July 2024, date of publication 29 July 2024, date of current version 7 August 2024.

Digital Object Identifier 10.1109/ACCESS.2024.3435515

RESEARCH ARTICLE

Accurate Fault Location Algorithm for Untransposed Transmission Lines Based on Network Phasor Equations in Positive-, Negative-, and Zero-Sequences Domain During Fault

MAHYAR ABASI
Department of Electrical Engineering, Faculty of Engineering, Arak University, Arak 38156-88349, Iran
Research Institute of Renewable Energy, Arak University, Arak 38156-88349, Iran
e-mail: m-abasi@araku.ac.ir

ABSTRACT The tower structure and geometrical arrangement of transmission line conductors in the power system depend on various technical, economic, and geographical factors and the age of construction of the lines. Thus, the arrangement of lines may not be transposed or follow the standards of the electricity industry. The untransposed conductors cause asymmetric couplings in the transmission lines, directly leading to destructive effect on the function of distance protection and accurate determination of the fault location. Fault location in untransposed transmission lines is presented as a novel research piece by investigating the circuit equations of positive-negative-zero sequences and using synchronous voltage measurements taken from the near and far terminals of the transmission line together with measuring the current of one terminal. In this algorithm, the effect of mutual interphase impedance and admittance due to the untransposed structure of the line is fully taken into account. Fault location equations are designed based on the complete equivalent circuit of the untransposed transmission line using the modeling of all effective parameters. As the presented design adopts the current measurements of one terminal, the destructive effect of the current measurement systems is dropped. The Simulink model of the suggested design has been implemented in Digsilent Power Factory software and the algorithm has been programmed in MATLAB software. The performance of the proposed algorithm has been tested and evaluated for a two-terminal network in normal and critical fault conditions, as well as for a 39-bus untransposed New England network. According to the obtained results, the average estimation error of all scenarios is approximately equal to 0.07%. The results presented in the simulation and sensitivity analysis section confirm the accurate and correct performance of the algorithm.

INDEX TERMS Fault location, normal shunt faults, positive, negative, and zero sequences, untransposed transmission lines.

NOMENCLATURE

Variable	Description
Z_{abc}	Impedance matrix of three phases of a, b, and c
Z_{ij}	Mutual impedance between phases i, j = a, b, c
Z_{ii}	Self-impedance of phase i, where i = a, b, c
$Z_{AB}^{(i,j)}$	Mutual impedance between sequences i and j and between points A and B
Z_{012}	Impedance matrix of 012-sequence
Z_i	Thevenin impedance of terminal i in the single-line diagram
Y_{abc}	Admittance matrix of three phases of a, b, and c

The associate editor coordinating the review of this manuscript and approving it for publication was Arturo Conde.

Y_{ij}	Mutual admittance between phases i, j = a, b, c
Y_{ii}	Self-admittance of phase i, where i = a, b, c
$Y_{AB}^{(i,j)}$	Mutual admittance between sequences i and j and between points A and B
Y_{012}	Admittance matrix of 012-sequence
Y_i	Thevenin admittance of terminal i in the single-line diagram
$I_F^{(i)}$	The *i*th sequence current of point A
$I_R^{(i)}$	The *i*th sequence current of terminal R
$I_S^{(i)}$	The *i*th sequence current of terminal S
$V_F^{(i)}$	The *i*th sequence voltage of point A
$V_R^{(i)}$	The *i*th sequence voltage of terminal R
$I_S^{(i)}$	The *i*th sequence current of terminal S
$V_F^{(i)}$	The *i*th sequence voltage of point A
$V_R^{(i)}$	The *i*th sequence voltage of terminal R
$V_S^{(i)}$	The *i*th sequence voltage of terminal S
$V_{RF}^{(i)}$	The *i*th sequence voltage of the fault point from terminal R side
$V_{SF}^{(i)}$	The *i*th sequence voltage of the fault point from terminal S side
Vk	Voltage of terminal K in the single-line diagram
ri	Resistance of transmission line
$Cabc$	Capacitance matrix of three phases of a, b, and c
ω	System angular frequency
$GMRi$	Geometric mean radius of conductor i
Dij	Distance between conductors i and j
Sij	Distance between conductor i and image j
T	Fortescue transform matrix
$L_F^{(acu)}$	The actual distance of fault point from terminal S
$L_F^{(cal)}$	The calculated distance of fault point from terminal S
L_T	Total length of the transmission line under study

I. INTRODUCTION

A. RESEARCH MOTIVATION AND NECESSITY

Accurate estimation of fault location in long transmission lines (TLs) and eliminating its cause are among the main challenges of the TL's incident team. If fault location estimation using the fault location algorithms is not performed correctly and is prone to errors, it will increase the blackout duration and lead to many operation consequences. Normally, the structure and arrangement of the cross-arms of TL towers are triangular and this makes the distance of three phase conductors mutually equal, which is known as transposed transmission lines. Nonetheless, if the distances between mutual phases are not equal, this leads to different values of impedance and inductive admittance parameters between the phases, as well as asymmetric structure of the line, which ultimately produces unequal mutual impedance and admittance components for positive, negative, and zero-sequence (PNZS). The production of these components strongly affects the line distance protection algorithms that are dependent on PNZS, and if the transposed line protection algorithms are used for untransposed lines, then the result of fault location will be very erroneous. To deal with this challenge, it is advised to design fault location algorithms for untransposed transmission lines. Therefore, according to the mentioned challenges and the fact that the basis of the logic of comprehensive distance protection designs is based on the PNZS line, the best option is to design a fault location algorithm in untransposed lines based on the analysis of PNZS phasor equations. In this modeling, since the full effect of all the mutual components of the sequences can be seen in the circuit model and all the equations are projected based on these parameters, this method is very accurate and efficient in terms of estimation accuracy. In the following, all the articles published in the field of fault location for untransposed transmission lines have been fully reviewed chronologically.

B. LITERATURE REVIEW

In 1990, for the first time, a plan for fault location in untransposed TLs was presented using the information about synchronous current and voltage from both ends of TLs [1]. The plan calculated the fault location by solving the phasor equation of the fault point voltage calculated from two terminals to the fault point. Two years later, Girgis et al. [2] extended the algorithm presented in [1] to three-terminal untransposed TLs using asynchronous data. In continuation of the studies conducted in [2], the idea of fault location in untransposed double-circuit TLs using the methods of eigenvalue/eigenvector theory to separate the effects of mutual coupling between parallel lines, common-differential component network analysis, and impedance equation analysis of the faulty network was presented in [3], [4], and [5], respectively. After the publication of various articles in this field, fault location in untransposed TLs with special topologies has attracted the attention of scholars [6], [7]. Reference [6] discussed an algorithm that adopts current and voltage phasors for fault location in untransposed four-circuit parallel TLs using the measured information taken from one side of the TL for single-circuit and inter-circuit faults. In [7], a fault location algorithm in untransposed multi-terminal TLs was presented. In this design, by using a search method for optimization and minimization of an objective function, the possible location of the fault in all parts was examined and then the exact solution was calculated. Then, in the years 2013 to 2016, the method of calculating the fault location in untransposed TLs using impedance and admittance matrix analysis was proposed [8], [9], [10]. In [8], a new algorithm to locate faults in untransposed TLs was presented using the impedance matrix analysis of TLs and the data of both

terminals. Reference [9] presented a fault location method through the wide-area analysis of the network impedance matrix using synchronous current and voltage phasors and assuming zero reactive power consumption at the fault location. The method can be implemented in any type of transposed/untransposed lines regardless of the arrangement of the lines. In [10], the fault location method was presented for TLs with flat or triangular towers with symmetric impedance and admittance matrices. The algorithm was based on current and voltage phasors for high-voltage transmission networks, including untransposed single-circuit overhead lines with horizontal arrangement of phase conductors. Further, in [11], the fault location approach was presented to deal with faults occurring in untransposed TLs based on the least square error method to solve the phasor equations of three-phase voltages and currents at line terminals. Then, the theory of using the Taylor series expansion of distributed-parameters line model to locate faults in three-terminal [12] and four-circuit [13] TLs for different kinds of normal shunt faults, developing faults, and cross-country faults was presented. The methods that have been reviewed so far all depend on TL parameters and data; therefore, to reduce this sensitivity and dependence, researchers have presented several algorithms [16], [17], [18], which are independent of line parameters when finding fault regions in untransposed TLs. Reference [14] introduced an algorithm to locate faults on untransposed TLs based on asynchronous data obtained from both sides of the line and without the need for line parameter information. In [15], a method independent of line parameters data was presented for fault location in untransposed TLs with asymmetric tower structure, which required Synchrophasor measurements of voltage and current of the two ends of the line for implementation. Reference [16] discussed a parameter-free fault location algorithm for transposed TLs based on phasor theory. In [17], the fault location algorithm for untransposed three-terminal TLs independent of TL parameter information and using the phasor analysis was presented. Reference [18] discussed a non-iterative algorithm with the aim of identifying the fault area in transposed TLs without TL parameters. Reference [19] presented the fault location algorithm in untransposed double-circuit TLs based on time domain equations for phase-to-phase and phase-to-ground inter-circuit faults. For fault location in this proposed method, a linear combination of time domain equations is presented as an adaptive linear combination with window inputs. A fault location method in transposed and untransposed TLs based on analyzing current and voltage phasor equations of the fault point as well as the network impedance and admittance matrix was introduced in [19]. The proposed method uses the calculation of the fault current based on the equations governing the fault point to find the location and resistance of the fault. In literature [20], a fault location method for transposed TLs based on phasor equations and asynchronous data transmission from both sides of the line was presented. The method was designed for a case where the phase shift operation has been performed at three different distances in an untransposed structure, and the entire line is considered as transposed, but during the sections, its structure is as untransposed. Reference [21] proposed a fault location method for untransposed hybrid double-circuit transmission lines with a T-off joint. The method adopts the phasor equations governing the fault point and non-synchronous current and voltage data of all three terminals to find the faulty section.

According to the above literature, the research gap of this topic is as follows:

- Using new techniques and formulations that are not in the form of fault location designs in distance relays and require a separate processor.
- Failure to provide a comprehensive formulated method to analyze all 10 different types of shunt fault modes
- Dependence of some methods on the network impedance and admittance matrix model
- Dependence of some methods on complete current and voltage data on both sides of the line, synchronously or asynchronously
- Dependence of some methods on optimization and search-oriented methods without providing detailed mathematical analysis
- Dependence of some proposed methods on line topology and network structure

C. CONTRIBUTIONS

A fault location scheme is proposed in the present research as a novel idea for untransposed TLs based on the analysis of circuit equations of positive-negative-zero sequences (PNZS). In this method, to solve the problem, first, an accurate model of the faulty circuit is presented by considering the mutual impedance and admittance of the phases and the ground for untransposed TLs in the PNZS domain. Then, the fault points current and voltage equations have been expanded according to the detailed modeling mentioned in the foregoing part, and finally, the location of the fault has been calculated using the fault boundary condition equations. Also, the suggested approach depends on synchronous voltage phasor measurements taken from both terminals of the TL and from the current data of only one side of the line. The network under test was modeled in Digsilent software and the proposed algorithm was programmed in an M-file MATLAB environment. The method presented in this paper is significantly accurate as it incorporates a precise new modeling, and the fault location estimation error in its calculation results is negligible.

D. PAPER ORGANIZATION

Following the foregoing introduction provided concerning the area under discussion, Section II present the proposed algorithm. Section III describes the software simulation and analysis of the results. In Section IV, the sensitivity of the algorithm to critical and special conditions is examined. In Section V, there is a discussion and comparison between

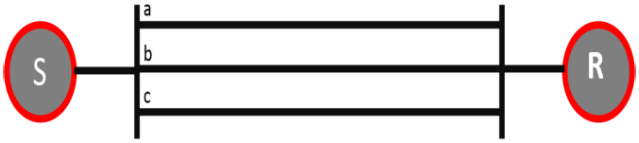

FIGURE 1. Three-phase circuit of untransposed three-phase TL between S and R stations.

the results of this study and the reference literature. Next, in Section VI, the conclusion is provided, and finally, the appendices are presented at the end of the paper.

II. THE PROPOSED ALGORITHM

A. THE SYSTEM UNDER STUDY

This subsection presents the formulation governing the faulty circuit in the domain of PNZS in an untransposed TL to find the fault point or area. The topology of the desired line is given in Fig. 1. All the line transmission towers considered between S and R stations are in the form of flat towers considered in Fig. 2. According to the arrangement of the three-phase conductors between S and R stations, the arrangement of the conductors is horizontal, and this has caused the distance of all three conductors to be different from each other.

In this topology, it is assumed that the three-phase voltages of both stations and the three-phase current of station S during the fault event (from fault occurrence to fault clearance by breakers, which is usually about 3 cycles) are received by voltage transformers. Then PMUs calculate the phasor values and GPS synchronizes these quantities. Next, the phasor values calculated from the voltages are transferred to the domain of PNZS by the Fortescue transform matrix. Also, in this paper, it is assumed that before locating the fault, the stages of detecting the occurrence of the fault and faulty phase have been carried out and are known in advance. At this stage, the only goal is to locate the fault occurring in the faulty phase(s). One assumption taken in the present study is that the faulty impedance is of resistive type and its reactance is assumed to be zero. Also, as a hypothesis, it should be mentioned in this section that the adopted equations can determine the location of all normal shunt faults (ten types of faults).

B. MODELING THE UNTRANSPOSED TL

Untransposed TLs have electric and magnetic coupling parameters between phases, so their modeling is different from transposed lines. Their lack of accurate modeling leads to erroneous functions of distance protection and fault location. Therefore, in this part, the goal is to accurately model these types of lines using the basic parameters of power systems. Fig. 3 shows the pi model of an untransposed TL in the abc domain.

According to Fig. 3, the impedance and admittance matrices of the untransposed network can be defined as

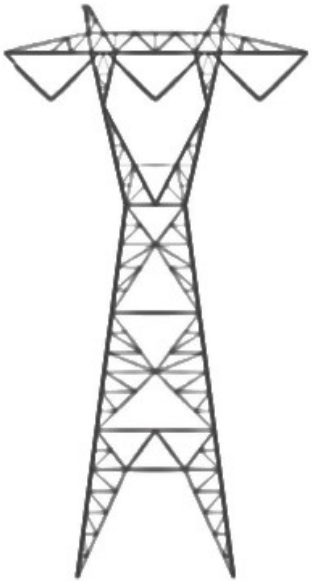

FIGURE 2. Flat tower structure considered between S and R stations.

Equations (1) and (2), respectively.

$$Z_{abc} = \begin{bmatrix} Z_{aa} & Z_{ab} & Z_{ac} \\ Z_{ba} & Z_{bb} & Z_{bc} \\ Z_{ca} & Z_{cb} & Z_{cc} \end{bmatrix} \tag{1}$$

$$Y_{abc} = \begin{bmatrix} Y_{aa} & Y_{ab} & Y_{ac} \\ Y_{ba} & Y_{bb} & Y_{bc} \\ Y_{ca} & Y_{cb} & Y_{cc} \end{bmatrix} \tag{2}$$

The relationships presented in Equation (3) can be used to obtain the components of the impedance matrix:

$$Z_{abc} = \begin{cases} Z_{ii} = r_i + 0.0953 \\ \qquad +j\,0.12134\ [\ln(\dfrac{1}{GMR_i}) + 7.93402]\ \Omega/mile \\ Z_{ij} = 0.0953 \\ \qquad +j\,0.12134\ [\ln(\dfrac{1}{D_{ij}}) + 7.93402]\ \Omega/mile \\ i, j = a, b, c \end{cases} \tag{3}$$

Equation (4) can also be used to calculate the coefficients of the admittance matrix:

$$Y_{abc} = j\,\omega\ [C_{abc}] \tag{4}$$

so that $[C_{abc}] = [P_{abc}]^{-1}$ and elements of P_{abc} matrix can be calculated from the relations presented in Equation (5):

$$P_{abc} = \begin{cases} P_{ii} = 11.17689\ \ln(\dfrac{S_{ii}}{RD_i})\ mile/\mu i \\ P_{ij} = 11.17689\ \ln(\dfrac{S_{ij}}{D_{ij}})\ mile/\mu i \\ i, j = a, b, c \end{cases} \tag{5}$$

After calculating the impedance and admittance matrices of untransposed TLs in the domain of PNZS, we can convert

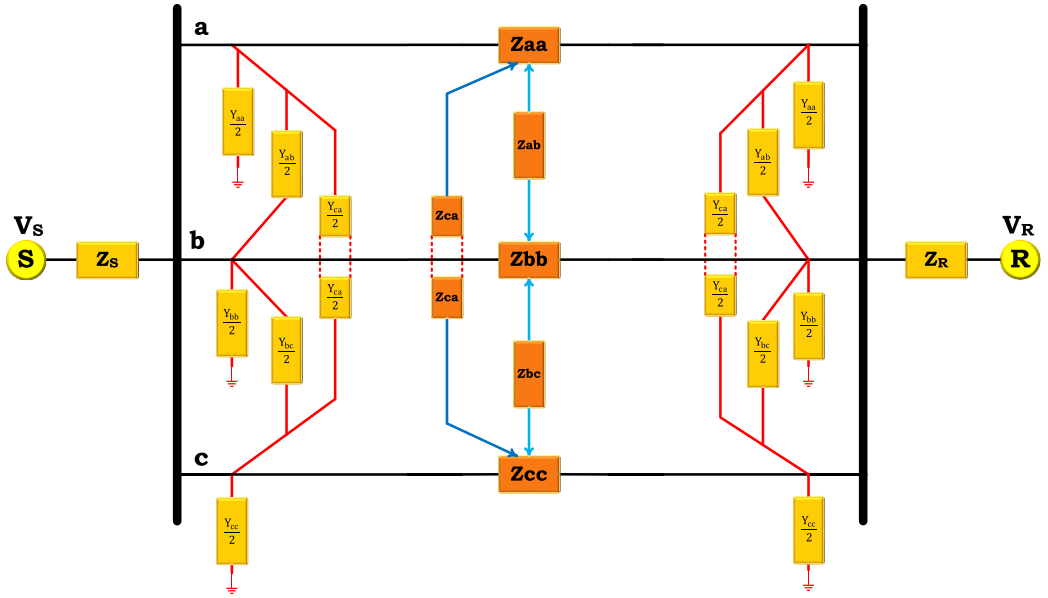

FIGURE 3. The phasor model of the untransposed TL in the normal operation mode in the *abc* sequence domain.

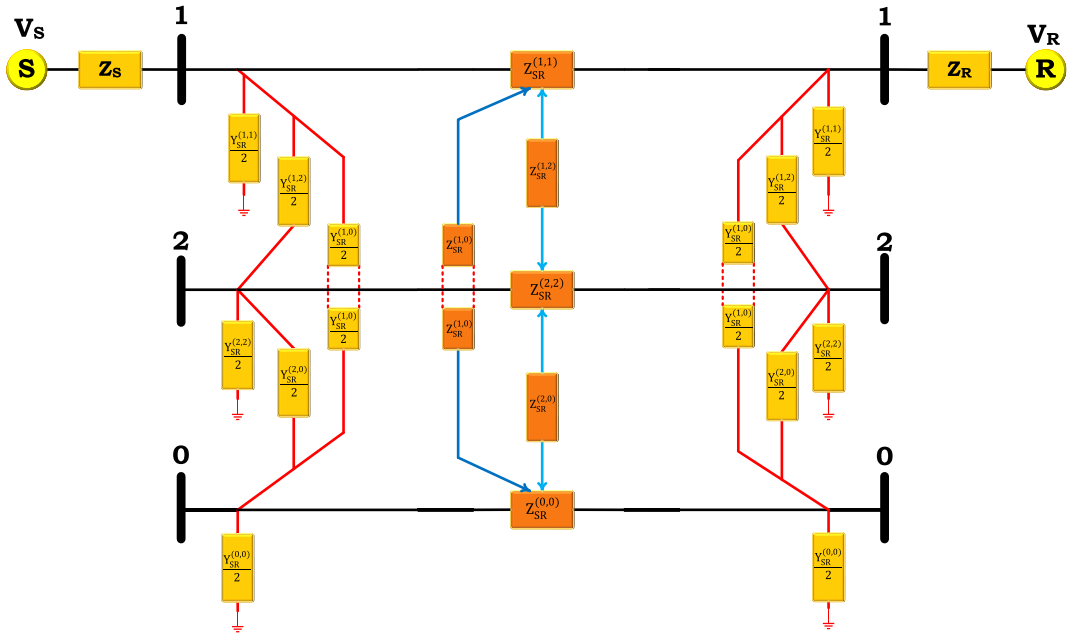

FIGURE 4. The phasor model of the untransposed TL in normal operation mode in the domain of PNZS.

these two matrices from the abc-sequence domain to the PNZS domain by using the Fortescue transform, as given in Equation (6):

$$\begin{cases} Z_{012} = T\ Z_{abc}\ T^{-1} \\ Y_{012} = T\ Y_{abc}\ T^{-1} \\ T = \dfrac{1}{3}\begin{bmatrix} 1 & 1 & 1 \\ 1 & \alpha & \alpha^2 \\ 1 & \alpha^2 & \alpha \end{bmatrix} \\ \alpha = 1\angle 120^o \end{cases} \tag{6}$$

In the case of untransposed lines, the circuits of PNZS are independent of each other, but in untransposed lines, these circuits have magnetic and electrical linking and coupling with each other in the normal network state without faults. Hence, the circuit equivalent in Fig. 3 can be depicted in the domain of PNZS during normal conditions, as shown in Fig. 4.

C. CALCULATING THE FAULTY POINT CURRENT AND VOLTAGE IN THE PNZS DOMAIN

A fault is assumed to occur at point F and at a distance of L_{SF}, one kilometer away from terminal S. By using the KVL

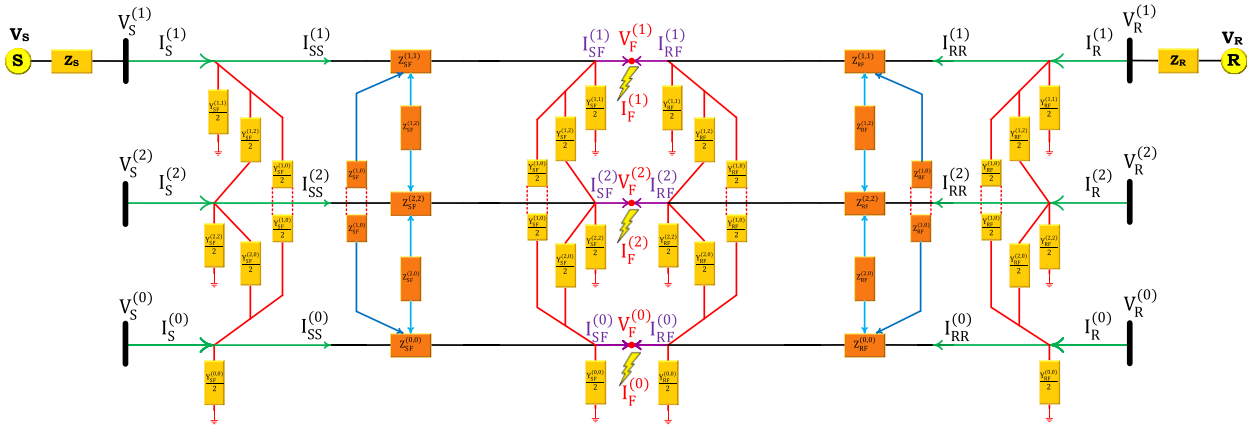

FIGURE 5. Phasor model of the faulty untransposed TL in the PNZS domain.

and KCL equations governing the circuit, the currents and voltages of each of PNZS, the fault point can be identified. All the currents and voltages inside all three circuits are expressed based on those of the three terminals in PNZS. The A_i coefficients can be found in Appendix A.

The current of each sequence of the fault point is found based on the current and voltage of all three sequences of terminals using the matrix presented in Equation (7), as shown at the bottom of the next page.

The voltage equation of all three sequences of the fault point is extracted based on the voltages and currents of all three sequences from both sides of the line terminals using Equations (8) and (9), as shown at the bottom of the next page. These two equations are equal to each other because they show the voltage of the fault point, but each of them is written based on the voltage drop equations of one side of the line.

D. SOLVING THE EQUATIONS OF BOUNDARY CONDITIONS FOR DIFFERENT SHUNT FAULTS

The conventional form of the boundary condition equation at the fault point for various shunt faults is as Equation (10). According to the type of fault, all the constant coefficients of this equation are given in Table 1.

$$K_{V\_1}\,V_F^{(1)} + K_{V\_2}\,V_F^{(2)} + K_{V\_0}\,V_F^{(0)} = R_F(K_{I\_1}\,I_F^{(1)} + K_{I\_2}\,I_F^{(2)} + K_{I\_0}\,I_F^{(0)}) \tag{10}$$

E. FAULT LOCATION AND ALGORITHM

To calculate the fault location, the boundary condition equation can be used; nevertheless, since the currents of all three sequences are not available on terminal R, voltage equations of the fault point given in matrix Equations (8) and (9) are used along with boundary condition equation to identify the fault location. The unknowns of this analysis include the fault resistance, the distance of the fault location, and the magnitude and angle of the currents of all three sequences of terminal R, which can be defined as variables R_F, L_{SF}, I_1, I_2, I_0, α_1, α_2, and α_0, respectively. The number of unknowns in the fault location equation is eight. So, to calculate L_{SF}, eight real independent equations or four imaginary equations are needed. These eight equations can be obtained from four imaginary equations.

- **Equation 1:** Equalization of the positive sequence voltage of the fault point from the two imaginary equations presented in the matrix Equations (8) and (9). This equation includes two real equations:

$$V_{RF}^{(1)} = V_{SF}^{(1)} \tag{11}$$

- **Equation 2:** Equalization of negative sequence voltage of the fault point from the two imaginary equations presented in the matrix Equations (8) and (9). This equation includes two real equations:

$$V_{RF}^{(2)} = V_{SF}^{(2)} \tag{12}$$

- **Equation 3:** Equalization of zero sequence voltage of the fault point from the two imaginary equations presented in the matrix Equations (8) and (9). This equation includes two real equations:

$$V_{RF}^{(0)} = V_{SF}^{(0)} \tag{13}$$

- **Equation 4:** The boundary condition equation presented in Equation (10), which includes two real equations.

In general, eight equations and eight unknowns are obtained to find the faulty location. It should be noted that impedances and admittance in Ai coefficients are functions of L_{SF}. In the end, a flowchart used for solving the fault location problem in untransposed lines can be depicted in Fig. 6.

According to Fig. 6, the implementation process of the proposed algorithm is as follows. The algorithm receives a series of information offline in advance and the information is always available to the algorithm as the basic settings. The information includes the electrical parameters of the entire line, such as resistance, inductance, internal and mutual capacitance between phases, and the entire length of the transmission line (km). Then, in the next step, after it is determined

that a fault has occurred (it is assumed fault incident time is known), online information is required for fault location. The required online information includes the phasor of the synchronous three-phase voltages of both terminals and the three-phase current phasor of the local side for the last fault cycle. In the next step, the algorithm starts the calculations. The calculations apply the Fortescue transformation on the current and voltage phasors received from the terminals and initialize the A coefficients, which are given in the Appendix of the paper. After these steps, it is time to create the current and voltage equation of the fault point in the PNZS domain, which is obtained according to Equation s. (7), (11), (12), and (13). These equations include the parameters of A and the initialization of the currents and voltages of the PNZS of the terminals. After forming the current and voltage equations of PNZS, the necessary equations can be formed based on the tables of coefficients presented in Table 1 as well as the type of faulty phase provided by the fault classification unit by default to the algorithm. These equations include 3 PNZS voltage equations presented in Equations (11), (12), and (13), as well as the equation of the boundary condition corresponding to the faulty phase, which are four real-imaginary equations. Equalizing the real and imaginary units of the sides of each equation results in a total of eight equations. The unknowns of these equations include the distance of the fault location, the fault resistance, the size and angle of the current phasors of the PNZS of the remote bus, and finally the distance of the fault location is obtained from the local bus. Eventually, the obtained distance must be within the range of the line, and the fault resistance must be a real number. If the results are confirmed, the algorithm is terminated and the calculated distance is correct, otherwise, the algorithm returns to the start step.

III. SIMULATIONS AND RESULTS ANALYSIS

In this part, the goal is to test and evaluate the designed algorithm in a software simulation system. The considered test network includes a 200 km, 230 kV TL, and both terminals of the TL are modeled with Thevenin sources. The complete information on the TL under study, including the impedance and admittance matrix of the TLs, the length of the TL, and the data related to the Thevenin equivalent circuit on both ends of the line, are given in Appendix B. According to Fig. 7, the network model under study including the Thevenin sources and also the desired untransposed TL is modeled in Digsilent software. The fault location algorithm designed here was programmed in an M-file in the MATLAB software. To evaluate the algorithm, 44 fault scenar-

$$\begin{bmatrix} I_F^{(1)} \\ I_F^{(2)} \\ I_F^{(0)} \end{bmatrix} = \begin{bmatrix} A_{55} & A_{56} & A_{57} & A_{58} & A_{59} & A_{60} & A_{73} & A_{74} & A_{75} & A_{76} & A_{77} & A_{78} \\ A_{61} & A_{62} & A_{63} & A_{64} & A_{65} & A_{66} & A_{79} & A_{80} & A_{81} & A_{82} & A_{83} & A_{84} \\ A_{67} & A_{68} & A_{69} & A_{70} & A_{71} & A_{72} & A_{85} & A_{86} & A_{87} & A_{88} & A_{89} & A_{90} \end{bmatrix} \begin{bmatrix} V_R^{(1)} \\ V_R^{(2)} \\ V_R^{(0)} \\ I_R^{(1)} \\ I_R^{(1)} \\ I_R^{(1)} \\ V_S^{(1)} \\ V_S^{(2)} \\ V_S^{(0)} \\ I_S^{(2)} \\ I_S^{(2)} \\ I_S^{(0)} \end{bmatrix} \tag{7}$$

$$\begin{bmatrix} V_F^{(1)} = V_{RF}^{(1)} \\ V_F^{(2)} = V_{RF}^{(2)} \\ V_F^{(0)} = V_{RF}^{(0)} \end{bmatrix} = \begin{bmatrix} A_{19} & A_{20} & A_{21} & A_{22} & A_{23} & A_{24} \\ A_{25} & A_{26} & A_{27} & A_{28} & A_{29} & A_{30} \\ A_{31} & A_{32} & A_{33} & A_{34} & A_{35} & A_{36} \end{bmatrix} \begin{bmatrix} V_R^{(1)} \\ V_R^{(2)} \\ V_R^{(0)} \\ I_R^{(1)} \\ I_R^{(2)} \\ I_R^{(0)} \end{bmatrix} \tag{8}$$

$$\begin{bmatrix} V_F^{(1)} = V_{SF}^{(1)} \\ V_F^{(2)} = V_{SF}^{(2)} \\ V_F^{(0)} = V_{SF}^{(0)} \end{bmatrix} = \begin{bmatrix} A_{37} & A_{38} & A_{39} & A_{40} & A_{41} & A_{42} \\ A_{43} & A_{44} & A_{45} & A_{46} & A_{47} & A_{48} \\ A_{49} & A_{50} & A_{51} & A_{52} & A_{53} & A_{54} \end{bmatrix} \begin{bmatrix} V_S^{(1)} \\ V_S^{(2)} \\ V_S^{(0)} \\ I_S^{(1)} \\ I_S^{(2)} \\ I_S^{(0)} \end{bmatrix} \tag{9}$$

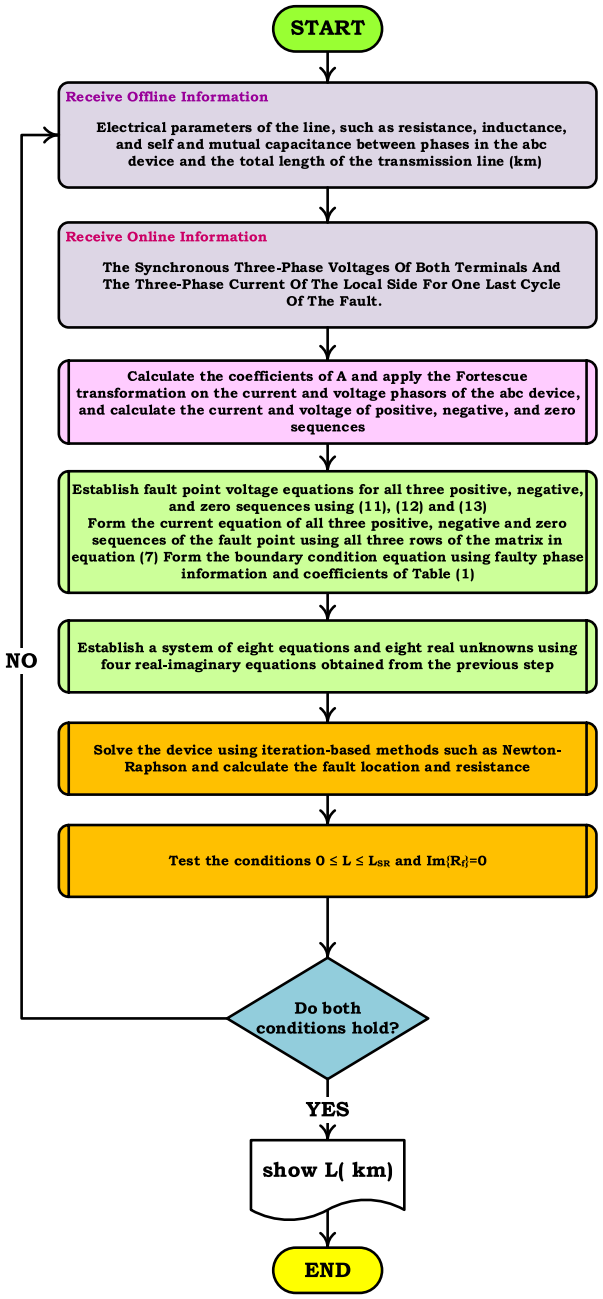

FIGURE 6. Flowchart of the complete design for fault location in untransposed TLs in the PNZS domain.

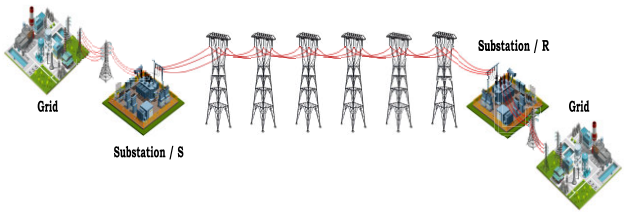

FIGURE 7. Modeled network under study.

ios in different locations and with different fault resistances have been used for all types of normal shunt faults. The

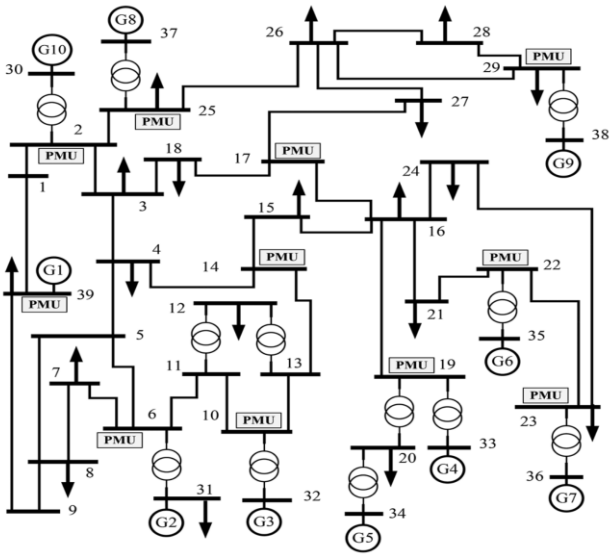

FIGURE 8. The 39-bus New England untransposed power system.

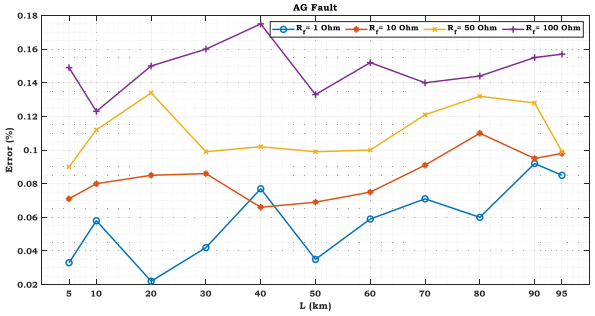

FIGURE 9. Error percentage of fault location estimation for an AG fault occurring at different places and resistance values.

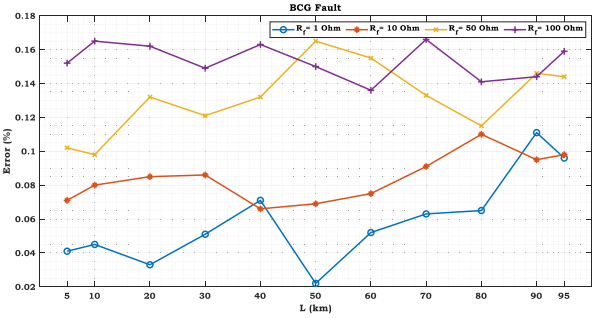

FIGURE 10. Error percentage of fault location estimation for a BCG fault occurring at different places and resistance values.

synchronous current and voltage sampled data by PMU with a sampling frequency of 2400 Hz are related to two post-fault cycles. These data have been sampled in phaser form and transferred from Digsilent software to the M-file environment of MATLAB software. Equation (14) has been used to evaluate the estimation error of fault location. All the information

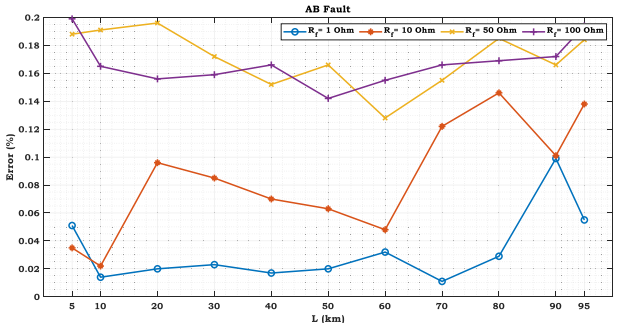

FIGURE 11. Error percentage of fault location estimation for an AB fault occurring at different places and resistance values.

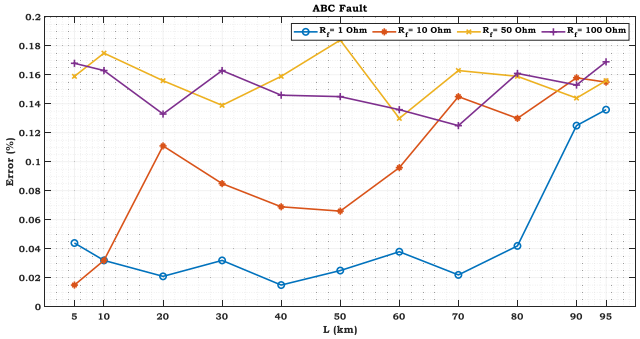

FIGURE 12. Error percentage of fault location estimation for an ABC fault occurring at different places and resistance values.

TABLE 1. Coefficients of the boundary condition equation for different normal shunt faults.

Eq. number	Type fault	K_{v_0}	K_{v_1}	K_{v_2}	K_{i_0}	K_{i_1}	K_{i_2}
I	AG	1	1	1	3	0	0
II	BG	1	a^2	a	3	0	0
III	CG	1	a	a^2	3	0	0
IV	ABG	0	1	-a	0	0	0
V	BCG	0	1	-1	0	0	0
VI	CAG	0	1	-a^2	0	0	0
VII	AB	0	1	-a	0	1	0
VIII	BC	0	1	-1	0	1	0
IX	CA	0	1	-a^2	0	1	0
X	ABC	0	1	0	0	1	0
XI	ABCG	0	1	0	0	1	0

related to the test scenarios along with the results obtained from the output of the algorithm are given in Table 2 in detail. According to the evaluation results, the significant difference in estimating the fault location is because of the 100 Ω fault CA occurring at 120 km far from terminal S, whose error value is +0.168% and this value is desirable and acceptable according to the error value presented in the previous references. The successfully obtained results validate the correct and accurate performance of the suggested algorithm.

$$erorr\% = \frac{L_F^{acu} - L_F^{Cal}}{L_T} \times 100 \tag{14}$$

TABLE 2. The results of testing different fault scenarios.

Type Fault	R_f (ohm)	Time(s)	$L_{S\text{-}F}$ Actual	$L_{S\text{-}F}$ Estimated	Error%
AG	1	0.10	100	99.96	+0.02
		0.15	20	19.85	0.075
	5	0.20	10	9.732	+0.134
		0.50	100	99.669	+0.165
	100	0.10	20	19.693	+0.153
		0.30	50	49.592	+0.204
BG	1	0.80	100	99.758	+0.121
		0.50	10	9.801	+0.099
	50	0.20	5	4.822	+0.089
		0.60	185	184.711	+0.144
	100	0.70	190	189.39	+0.305
		0.10	20	19.96	+0.02
CG	10	0.25	75	74.96	+0.020
		0.10	30	29.665	+0.167
	50	0.15	5	4.796	+0.102
		0.20	75	74.833	+0.083
	100	0.20	30	29.65	+0.175
		0.75	55	54.63	+0.185
ABG	5	0.10	30	29.91	+0.045
		0.15	50	49.863	+0.068
	10	0.20	80	79.801	+0.099
		0.50	5	3.903	+0.048
	100	0.10	55	54.59	+0.205
		0.30	100	99.69	+0.02
BCG	1	0.15	120	119.88	+0.060
		0.20	10	9.890	+0.055
	10	0.90	170	169.69	+0.155
		0.10	30	29.55	+0.225
	100	0.35	20	19.788	+0.106
		0.75	150	149.811	+0.094
CAG	1	0.25	55	54.63	+0.185
		0.10	5	4.69	+0.155
	20	0.15	175	174.799	+0.100
		0.20	130	129.881	+0.059
	100	0.20	10	9.882	+0.059
		0.75	190	189.716	+0.142
AB	1	0.80	5	4.9	+0.05
		0.50	50	49.56	+0.22
	50	0.20	75	75.172	-0.086
		0.60	150	150.22	-0.086
	100	0.70	4	4.162	-0.081
		0.10	130	130.232	-0.116
BC	1	0.25	50	50.193	-0.096
		0.10	175	175.173	-0.086
	10	0.15	100	100.267	-0.133
		0.20	195	195.291	-0.145
	100	0.20	25	24.66	+0.17
		0.75	35	34.85	+0.075
CA	5	0.10	135	135.277	-0.138
		0.15	5	5.168	-0.084
	50	0.20	50	50.22	-0.11
		0.50	10	10.16	-0.08
	100	0.10	120	120.336	-0.168
		0.30	10	10.255	-0.127
ABC	1	0.80	50	50.177	-0.088
		0.50	100	100.202	-0.101
	50	0.20	50	50.3	-0.15
		0.60	100	100.16	-0.05
	100	0.70	150	150.196	-0.098
		0.10	30	30.166	-0.083
ABCG	5	0.80	30	30.198	-0.099
		0.50	145	145.29	-0.145
	50	0.20	15	15.166	-0.083
		0.60	175	175.226	-0.113
	100	0.70	10	9.43	+0.285
		0.10	80	79.33	+0.335

Further, to examine the various dimensions of the proposed method, the formulation of fault location according to Fig. 8

TABLE 3. The algorithm test results for different sensitive and critical scenarios.

Scenario number	Title of sensitivity analysis	Description of sensitivity analysis scenario	L_{SF} Estimated	Error%
1	Analysis of the algorithm's sensitivity to the changes in series line impedance	In this scenario, the impedance of the positive and negative sequences of the line has increased by 10% and the impedance of the zero sequence has decreased by 5%. Also, if the value of the angle of each of the impedances is increased by 5 degrees compared to the actual value, it means that a 10 Ω AG fault has occurred at 50 km far from terminal S.	**48.89**	**0.55**
2	Analysis of sensitivity to the changes of mutual induction impedance between phases	In this scenario, it is assumed that the size of the mutual impedance between each two circuits increases by 5% and its angle increases by 10 degrees compared to the actual value. In this case, a 50 Ω BC fault has occurred at 150 km far from terminal S.	**150.21**	**-0.10**
3	Analysis of the algorithm's sensitivity to the changes in network frequency	In this scenario, it is assumed that the frequency of the Thevenin voltage source of terminal S fluctuates in the time interval of 1 s to 1.20 s with an oscillation period of 5 ms to the value of 2 Hz. Here, a solid three-phase fault appears in the time interval of 1.05 s to 1.20 s at 100 km away from terminal S.	**100.52**	**-0.26**
4	Analysis of sensitivity to the changes in line length	In this scenario, it is assumed that the length of the entire line has changed from 200 km to 300 km, and this value is given as input information to the algorithm. In this case, a CG fault with a resistance of 1 Ω has occurred at a distance of 75 km from terminal S.	**74.78**	**0.11**
5	Analysis of the algorithm's sensitivity to the out-of-synchronism of the two Thevenin sources and power swing	In this scenario, the angle of the Thevenin voltage source of terminal S relative to terminal R fluctuates by 30 degrees in the time interval of 1 s to 1.20 s with an oscillation period of 5 ms. Here, an ACG fault appears between 1.05 s and 1.20 s at 20 km away from terminal S.	**19.17**	**0.41**
6	Sensitivity of the algorithm to the appearance of a high-impedance fault	In this scenario, it is assumed that an AG fault with a resistance of 500 Ω has occurred at a distance of 50 km from terminal S.	**49.15**	**0.42**
7	Analysis of the algorithm's sensitivity to the data transfer delay	In this scenario, it is assumed that there is a delay of 1 ms in data transfer time by the PMU. Here, a 1 Ω BCG fault has occurred at 190 km away from terminal S.	**189.32**	**0.34**
8	Sensitivity of the algorithm to the current transformer fault	In this scenario, it is assumed that the magnitude of the measured current has decreased by 10% in the entire time period. In this case, a 100 Ω ABG fault has occurred at 20 km away from terminal S.	**18.98**	**0.51**
9	Sensitivity of the algorithm to the voltage transformer fault	In this case, the measured voltage magnitude has increased by 5% in the entire time period. Here, an AG fault appears at 170 km away from terminal S.	**170.69**	**0.34**
10	Sensitivity of the algorithm to the changes in the network Thevenin impedance	In this scenario, it is assumed that the value of the impedance of terminal S has increased by 5%. Here, a 5 Ω AC fault has occurred at 10 km away from terminal S.	**10.12**	**-0.06**

has been implemented on the 39-bus New England network with an untransposed structure. The complete information on the network is given in [22]. In this network, it is assumed that the fault occurred in the line between buses 22 and 23 at different distances with different resistances. The results of this implementation for AG, BCG, AB, and ABC faults are shown in Figs. 9 to 12, respectively.

IV. SENSITIVITY ANALYSIS

The results of testing the proposed algorithm in critical and sensitive conditions are given in Table 3. In this table, 10 sensitivity analysis scenarios were designed, and each of which was accurately modeled in Digsilent software. The results of fault location estimation and the algorithm error are provided separately for each scenario. According to the results presented in this table, the algorithm is the most sensitive to scenario (1) and the least sensitive to scenario (2).

V. DISCUSSION AND COMPARISON

Here, we compare the results of the suggested algorithm with those of the related literature. To this end and to make an accurate comparison, several indices can be incorporated. The findings of the comparison are tabulated in Table 4.

Index 1: This concerns the domain analysis of the problem. The domains of problem analysis include the impedance or phasor (Ph), traveling waves or time (TW), and artificial intelligence (AI).

Index 2: This indicator is related to data transfer, which includes data transfer in the synchronous mode (SY), the asynchronous mode (ASY), and the single-terminal mode (ST).

Index 3: It concerns the sampling frequency rate.

Index 4: This index concerns the dependency (DE) or independency (IND) of line parameters.

Index 5: It concerns the number of current and voltage measurements by the PMU. Each three-phase measurement of current (C) or voltage (V) is considered a measurement unit.

Index 6: This index is related to the type of problem solver and can be either iterative (IT) or non-iterative (NIT).

Index 7: This index is related to the evaluation of the practical implementation feasibility of the algorithms, which can be separated into three modes: hard (H), medium (M), and easy (E).

Index 8: This index is related to the number of network circuits (CI) under study.

TABLE 4. The results of comparing the proposed algorithm with algorithms presented in the literature.

Reference No	INDEXES									
	Index1	**Index2**	**Index3**	**Index4**	**Index5**	**Index6**	**Index7**	**Index8**	**Index9**	**Index10**
1	Ph	SY	NA	DE	C-V	NIT	E	1-CI	2-T	1.5%
2	Ph	ASY	NA	DE	C-V	IT	M	1-CI	3 and 2- T	0.05%
3	Ph	SY	3.84 kHz	IND	C-V	NIT	M	2-CI	2-T	0.1%
4	TW	SY	1MHz	DE	C-V	IT	H	1-CI	1-T	0.1%
5	Ph	------	7.76 kHz	DE	C-V	NIT	H	2-CI	1-T	0.85%
6	Ph	------	1kHz	DE	C-V	IT	H	4 -CI	1-T	0.1%
7	Ph	SY	NA	DE	C-V	NIT	M	1-CI	1 and 2-T	0.1%
8	Ph	ASY	NA	DE	C-V	IT	M	1-CI	2-T	1.2%
9	Ph	SY	NA	DE	C-V	IT	H	2-CI	2-T	0.2%
10	Ph	SY	NA	IND	C-V	NIT	H	1-CI	1-T	1%
11	Ph	SY	2.5 kHz	DE	C-V	IT	M	1-CI	2-T	0.05%
12	Ph	SY	2.5 kHz	DE	C-V	IT	H	2-CI	3-T	0.3%
13	Ph	SY	2.5 kHz	DE	C-V	IT	H	4-CI	2-T	0.3%
14	Ph	ASY	1kHz	DE	C-V	IT	H	2-CI	2-T	0.15%
15	Ph	SY	NA	DE	C-V	NIT	M	1-CI	2-T	0.03%
16	Ph	SY	NA	IND	C-V	NIT	H	1-CI	2-T	0.08%
17	Ph	SY	NA	DE	C-V	IT	H	1-CI	3-T	0.05%
18	Ph	ASY	4kHz	IND	C-V	NIT	H	1-CI	2-T	0.02%
19	TW	SY	NA	DE	C-V	NIT	H	2-CI	2-T	0.08%
20	Ph	------	NA	DE	C-V	IT	M	1-CI	2-T	0.1%
21	Ph	ASY	200kHz	DE	C-V	IT	H	1-CI	2-T	0.5%
22	Ph	ASY	100k Hz	DE	C-V	IT	M	2-CI	3-T	0.2%
Propose Method	Ph	SY	2.4kHz	DE	C-V	IT	M	1-CI	2-T	0.07%

Index 9: This index is related to the number of network terminals (T) under study.

Index 10: This concerns the average error of the simulation results

VI. CONCLUSION

The paper proposed a novel fault location algorithm for untransposed TLs using accurate modeling of the line in the PNZS domain. The line model is presented in the phasor domain and is based on accurate modeling of mutual impedances and admittances between the circuits of all three sequences. The formulation of fault location equations is based on the phasor equations governing the network for all types of normal shunt faults and no approximations have been used. The proposed algorithm incorporates the three-phase voltage of both terminals and the three-phase current of only one terminal to locate the fault. The algorithm's performance has been tested for 44 types of faults appearing at various areas and resistance values, and the average estimation error for these results is equal to 0.07% Also, according to the results provided in the sensitivity analysis section, the reliability of the algorithm has been tested and evaluated in different critical conditions, confirming its accurate performance. Due to the low sampling frequency rate and the high accuracy of the algorithm, it demonstrates a very suitable capability for practical implementation in the locators available in the industry.

APPENDICES

In this section, the appendices mentioned throughout the paper are provided. The first appendix is related to the coefficients given in Equations (7)-(9), and the second appendix concerns the test network information.

APPENDIX A
INFORMATION ON A_i COEFFICIENTS

$$A_1 = -((Y_{RF}^{(1,1)}/2) + (Y_{RF}^{(1,2)}/2) + (Y_{RF}^{(1,0)}/2))$$
$$A_2 = (Y_{RF}^{(1,2)}/2)$$
$$A_3 = (Y_{RF}^{(1,0)}/2)$$
$$A_4 = (Y_{RF}^{(2,1)}/2)$$
$$A_5 = -((Y_{RF}^{(2,1)}/2) + (Y_{RF}^{(2,2)}/2) + (Y_{RF}^{(2,0)}/2))$$
$$A_6 = (Y_{RF}^{(2,0)}/2)$$
$$A_7 = (Y_{RF}^{(0,1)}/2)$$
$$A_8 = (Y_{RF}^{(0,2)}/2)$$
$$A_9 = -((Y_{RF}^{(0,1)}/2) + (Y_{RF}^{(0,2)}/2) + (Y_{RF}^{(0,0)}/2))$$
$$A_{10} = -((Y_{SF}^{(1,1)}/2) + (Y_{SF}^{(1,2)}/2) + (Y_{SF}^{(1,0)}/2))$$
$$A_{11} = (Y_{SF}^{(1,2)}/2)$$
$$A_{12} = (Y_{SF}^{(1,0)}/2)$$
$$A_{13} = (Y_{SF}^{(2,1)}/2)$$
$$A_{14} = -((Y_{SF}^{(2,1)}/2) + (Y_{SF}^{(2,2)}/2) + (Y_{SF}^{(2,0)}/2))$$
$$A_{15} = (Y_{SF}^{(2,0)}/2)$$
$$A_{16} = (Y_{SF}^{(0,1)}/2)$$
$$A_{17} = -((Y_{SF}^{(0,1)}/2) + (Y_{SF}^{(0,2)}/2) + (Y_{SF}^{(0,0)}/2))$$
$$A_{18} = (Y_{SF}^{(0,2)}/2)$$

$$A_{19} = 1 - Z_{RF}^{(1,1)}A_1 - Z_{RF}^{(1,2)}A_4 - Z_{RF}^{(1,0)}A_7$$
$$A_{20} = -Z_{RF}^{(1,1)}A_2 - Z_{RF}^{(1,2)}A_5 - Z_{RF}^{(1,0)}A_8$$
$$A_{21} = -Z_{RF}^{(1,1)}A_3 - Z_{RF}^{(1,2)}A_6 - Z_{RF}^{(1,0)}A_9$$
$$A_{22} = -Z_{RF}^{(1,1)}$$
$$A_{23} = -Z_{RF}^{(1,2)}$$
$$A_{24} = -Z_{RF}^{(1,0)}$$
$$A_{25} = -Z_{RF}^{(2,1)}A_1 - Z_{RF}^{(2,2)}A_4 - Z_{RF}^{(2,0)}A_7$$
$$A_{26} = 1 - Z_{RF}^{(2,1)}A_2 - Z_{RF}^{(2,2)}A_5 - Z_{RF}^{(2,0)}A_8$$
$$A_{27} = -Z_{RF}^{(2,1)}A_3 - Z_{RF}^{(2,2)}A_6 - Z_{RF}^{(2,0)}A_9$$
$$A_{28} = -Z_{RF}^{(2,1)}$$
$$A_{29} = -Z_{RF}^{(2,2)}$$
$$A_{30} = -Z_{RF}^{(2,0)}$$
$$A_{31} = -Z_{RF}^{(0,1)}A_1 - Z_{RF}^{(0,2)}A_4 - Z_{RF}^{(0,0)}A_7$$
$$A_{32} = -Z_{RF}^{(0,1)}A_2 - Z_{RF}^{(0,2)}A_5 - Z_{RF}^{(0,0)}A_8$$
$$A_{33} = 1 - Z_{RF}^{(0,1)}A_3 - Z_{RF}^{(0,2)}A_6 - Z_{RF}^{(0,0)}A_9$$
$$A_{34} = -Z_{RF}^{(0,1)}$$
$$A_{35} = -Z_{RF}^{(0,2)}$$
$$A_{36} = -Z_{RF}^{(0,0)}$$
$$A_{37} = 1 - Z_{SF}^{(1,1)}A_{10} - Z_{SF}^{(1,2)}A_{13} - Z_{SF}^{(1,0)}A_{16}$$
$$A_{38} = -Z_{SF}^{(1,1)}A_{11} - Z_{SF}^{(1,2)}A_{14} - Z_{SF}^{(1,0)}A_{17}$$
$$A_{39} = -Z_{SF}^{(1,1)}A_{12} - Z_{SF}^{(1,2)}A_{15} - Z_{SF}^{(1,0)}A_{18}$$
$$A_{40} = -Z_{RF}^{(1,1)}$$
$$A_{41} = -Z_{RF}^{(1,2)}$$
$$A_{42} = -Z_{RF}^{(1,0)}$$
$$A_{43} = -Z_{SF}^{(2,1)}A_{10} - Z_{SF}^{(2,2)}A_{13} - Z_{SF}^{(2,0)}A_{16}$$
$$A_{44} = -Z_{SF}^{(2,1)}A_{11} - Z_{SF}^{(2,2)}A_{14} - Z_{SF}^{(2,0)}A_{17}$$
$$A_{45} = -Z_{SF}^{(2,1)}A_{12} - Z_{SF}^{(2,2)}A_{15} - Z_{SF}^{(2,0)}A_{18}$$
$$A_{46} = -Z_{SF}^{(2,1)}$$
$$A_{47} = -Z_{SF}^{(2,2)}$$
$$A_{48} = -Z_{SF}^{(2,0)}$$
$$A_{49} = -Z_{SF}^{(0,1)}A_{10} - Z_{SF}^{(0,2)}A_{13} - Z_{SF}^{(0,0)}A_{16}$$
$$A_{50} = -Z_{SF}^{(0,1)}A_{11} - Z_{SF}^{(1,2)}A_{14} - Z_{SF}^{(0,0)}A_{17}$$
$$A_{51} = -Z_{SF}^{(0,1)}A_{12} - Z_{SF}^{(0,2)}A_{15} - Z_{SF}^{(0,0)}A_{18}$$
$$A_{52} = -Z_{SF}^{(0,1)}$$
$$A_{53} = -Z_{SF}^{(0,2)}$$
$$A_{54} = -Z_{SF}^{(0,0)}$$
$$A_{55} = A_1 + A_1A_{19} + A_2A_{25} + A_3A_{31}$$
$$A_{56} = A_2 + A_1A_{20} + A_2A_{26} + A_3A_{32}$$
$$A_{57} = A_3 + A_1A_{21} + A_2A_{27} + A_3A_{33}$$
$$A_{58} = 1 + A_1A_{22} + A_2A_{28} + A_3A_{34}$$

TABLE 5. Information on Thevenin sources on both ends of the TL under study.

Parameter	Source 1	Source 2
V	$230\angle -20.8^{\circ}$ kV	$230\angle 9.2^{\circ}$ kV
X/R	10	10
r_1	0.8716 Ω	1.7431 Ω
r_0	1.3074 Ω	2.6147 Ω
l_1	0.02576 H	0.05154 H
l_0	0.00648 H	0.0129 H

$$A_{59} = A_1A_{23} + A_2A_{29} + A_3A_{35}$$
$$A_{60} = A_1A_{24} + A_2A_{30} + A_3A_{36}$$
$$A_{61} = A_4 + A_5A_{25} + A_4A_{19} + A_6A_{31}$$
$$A_{62} = A_5 + A_5A_{25} + A_4A_{20} + A_6A_{32}$$
$$A_{63} = A_6 + A_5A_{27} + A_4A_{21} + A_6A_{33}$$
$$A_{64} = A_4A_{28} + A_4A_{22} + A_6A_{34}$$
$$A_{65} = 1 + A_5A_{29} + A_4A_{23} + A_6A_{35}$$
$$A_{66} = A_5A_{30} + A_4A_{24} + A_6A_{36}$$
$$A_{67} = A_7 + A_9A_{31} + A_7A_{19} + A_8A_{25}$$
$$A_{68} = A_8 + A_9A_{32} + A_7A_{20} + A_8A_{26}$$
$$A_{69} = A_9 + A_9A_{33} + A_7A_{21} + A_8A_{27}$$
$$A_{70} = A_9A_{34} + A_7A_{22} + A_8A_{28}$$
$$A_{71} = A_9A_{35} + A_7A_{23} + A_8A_{29}$$
$$A_{72} = 1 + A_9A_{36} + A_7A_{24} + A_8A_{30}$$
$$A_{73} = A_{10} + A_{10}A_{37} + A_{11}A_{43} + A_{12}A_{49}$$
$$A_{74} = A_{11} + A_{10}A_{38} + A_{11}A_{44} + A_{12}A_{50}$$
$$A_{75} = A_{12} + A_{10}A_{39} + A_{11}A_{45} + A_{12}A_{51}$$
$$A_{76} = 1 + A_{10}A_{40} + A_{11}A_{46} + A_{12}A_{52}$$
$$A_{77} = A_{10}A_{41} + A_{11}A_{47} + A_{12}A_{53}$$
$$A_{78} = A_{10}A_{42} + A_{11}A_{48} + A_{12}A_{54}$$
$$A_{79} = A_{13} + A_{14}A_{43} + A_{13}A_{37} + A_{15}A_{49}$$
$$A_{80} = A_{14} + A_{14}A_{44} + A_{13}A_{38} + A_{15}A_{50}$$
$$A_{81} = A_{15} + A_{14}A_{45} + A_{13}A_{39} + A_{15}A_{51}$$
$$A_{82} = A_{14}A_{46} + A_{13}A_{40} + A_{15}A_{52}$$
$$A_{83} = 1 + A_{14}A_{47} + A_{13}A_{41} + A_{15}A_{53}$$
$$A_{84} = A_{14}A_{48} + A_{13}A_{42} + A_{15}A_{54}$$
$$A_{85} = A_{16} + A_{17}A_{49} + A_{16}A_{37} + A_{18}A_{43}$$
$$A_{86} = A_{17} + A_{17}A_{50} + A_{16}A_{38} + A_{18}A_{44}$$
$$A_{87} = A_{18} + A_{17}A_{51} + A_{16}A_{39} + A_{18}A_{45}$$
$$A_{88} = A_{17}A_{52} + A_{16}A_{40} + A_{18}A_{46}$$
$$A_{89} = A_{17}A_{53} + A_{16}A_{41} + A_{18}A_{47}$$
$$A_{90} = 1 + A_{14}A_{54} + A_{16}A_{42} + A_{18}A_{48}$$

APPENDIX B

The information related to the Thevenin sources on both ends of the TL is given in Table 5 and the data of the impedance and admittance matrices of the lines in the three-phase

abc domain is expressed in Equations (15) and (16), respectively.

$$Z_{abc} = \begin{bmatrix} 0.1106 + j0.7149 & 0.0457 + j0.3645 & 0.0457 + j0.3210 \\ 0.0457 + j0.3645 & 0.1106 + j0.7149 & 0.0457 + j0.3645 \\ 0.0457 + j0.3210 & 0.0457 + j0.3645 & 0.1106 + j0.7149 \end{bmatrix}^{\Omega/km} \quad (15)$$

$$Y_{abc} = \begin{bmatrix} j2.4735 & -j0.7588 & -j0.4374 \\ -j0.7588 & j2.629 & -j0.7588 \\ -j0.4374 & -j0.7588 & j2.4735 \end{bmatrix}^{/km} \quad (16)$$

REFERENCES

[1] A. T. Johns and S. Jamali, "Accurate fault location technique for power transmission lines," *IEE Proc. C Gener., Transmiss. Distribution*, vol. 137, no. 6, p. 395, 1990.
[2] A. A. Girgis, D. G. Hart, and W. L. Peterson, "A new fault location technique for two- and three-terminal lines," *IEEE Trans. Power Del.*, vol. 7, no. 1, pp. 98–107, Jan. 1992.
[3] C.-S. Chen, C.-W. Liu, and J.-A. Jiang, "A new adaptive PMU based protection scheme for transposed/untransposed parallel transmission lines," *IEEE Trans. Power Del.*, vol. 17, no. 2, pp. 395–404, Apr. 2002.
[4] G. Song, J. Suonan, Q. Xu, P. Chen, and Y. Ge, "Parallel transmission lines fault location algorithm based on differential component net," *IEEE Trans. Power Del.*, vol. 20, no. 4, pp. 2396–2406, Oct. 2005.
[5] S.-H. Kang, Y.-J. Ahn, Y.-C. Kang, and S.-R. Nam, "A fault location algorithm based on circuit analysis for untransposed parallel transmission lines," *IEEE Trans. Power Del.*, vol. 24, no. 4, pp. 1850–1856, Oct. 2009.
[6] E. E. Ngu, K. Ramar, and A. Eisa, "One-end fault location method for untransposed four-circuit transmission lines," *Int. J. Electr. Power Energy Syst.*, vol. 43, no. 1, pp. 660–669, Dec. 2012.
[7] S. G. Di Santo and C. E. M. Pereira, "Fault location method for untransposed transmission lines with derivations," in *Proc. PES T&D*, Orlando, FL, USA, May 2012, pp. 1–8.
[8] D. A. G. Vieira, D. B. Oliveira, and A. C. Lisboa, "A closed-form solution for untransposed transmission-lines fault location with nonsynchronized terminals," *IEEE Trans. Power Del.*, vol. 28, no. 1, pp. 524–525, Jan. 2013.
[9] X. Jiao and Y. Liao, "Accurate fault location for untransposed/transposed transmission lines using sparse wide-area measurements," *IEEE Trans. Power Del.*, vol. 31, no. 4, pp. 1797–1805, Aug. 2016.
[10] A. S. Dobakhshari, "Noniterative parameter-free fault location on untransposed single-circuit transmission lines," *IEEE Trans. Power Del.*, vol. 32, no. 3, pp. 1636–1644, Jun. 2017.
[11] S. Azizi, M. Sanaye-Pasand, and M. Paolone, "Locating faults on untransposed, meshed transmission networks using a limited number of synchrophasor measurements," *IEEE Trans. Power Syst.*, vol. 31, no. 6, pp. 4462–4472, Nov. 2016.
[12] A. Saber, A. Emam, and H. Elghazaly, "New fault location scheme for three-terminal untransposed parallel transmission lines," *Electric Power Syst. Res.*, vol. 154, pp. 266–275, Jan. 2018.
[13] A. Saber, "New fault location scheme for four-circuit untransposed transmission lines," *Int. J. Electr. Power Energy Syst.*, vol. 99, pp. 225–232, Jul. 2018.
[14] C. A. Apostolopoulos and G. N. Korres, "A novel algorithm for locating faults on transposed/untransposed transmission lines without utilizing line parameters," *IEEE Trans. Power Del.*, vol. 25, no. 4, pp. 2328–2338, Oct. 2010.
[15] W. Zhu, Y. Liu, D. Lu, and X. Zheng, "A novel phasor domain parameter-free fault location algorithm on untransposed transmission lines," in *Proc. IEEE 8th Int. Conf. Adv. Power Syst. Autom. Protection (APAP)*, China, Oct. 2019, pp. 1662–1666.
[16] D. Lu, Y. Liu, B. Xie, R. Fan, and L. Sun, "An improved phasor domain parameter-free fault location algorithm on untransposed lines," in *Proc. IEEE/PES Transmiss. Distribution Conf. Exposit. (T&D)*, Chicago, IL, USA, Oct. 2020, pp. 1–5.
[17] D. Lu, Y. Liu, and D. Lu, "An iterative parameter-free fault location method on three-terminal untransposed transmission lines," in *Proc. IEEE Power Energy Soc. Gen. Meeting (PESGM)*, Montreal, QC, Canada, Aug. 2020, pp. 1–5.
[18] D. Lu, Y. Liu, S. Chen, B. Wang, and D. Lu, "An improved noniterative parameter-free fault location method on untransposed transmission lines using multi-section models," *IEEE Trans. Power Del.*, vol. 37, no. 3, pp. 1356–1369, Jun. 2022.
[19] H. Abdollahzadeh, "A distance protection approach for untransposed parallel transmission lines in case of phase-phase-ground inter-circuit faults," *Int. J. Electr. Power Energy Syst.*, vol. 145, Feb. 2023, Art. no. 108623.
[20] D. Lu, Y. Liu, Y. Xie, Y. Zhu, and R. Fan, "An accurate unsynchronized fault location method on practically transposed transmission lines with closed-form solutions," *Int. J. Electr. Power Energy Syst.*, vol. 155, Jan. 2024, Art. no. 109522.
[21] S. Anand, K. Kalita, S. K. Parida, and B. R. Bhalja, "An integrated backup protection and fault location module for unsynchronized three-terminal multisection hybrid transmission lines," *Electric Power Syst. Res.*, vol. 233, Aug. 2024, Art. no. 110491.
[22] *DIgSILENT Power Factory*, Version 14, DIgSILENT, Gomaringen, Germany, 2008.

MAHYAR ABASI was born in Iran, in 1989. He received the Ph.D. degree in electrical power engineering from Shahid Chamran University of Ahvaz, Ahvaz, Iran, in 2021. He is currently an Assistant Professor with the Electrical Engineering Department, Arak University, Arak, Iran. In 2021, he was introduced as the top researcher of Khuzestan Province, Iran. From 2021 to 2023, he successfully received four titles from the membership schemes of the National Elite Foundation in Iran. His research background is more than 60 published journal and conference papers, more than ten authored books, 11 industrial research projects, and a patent in power systems. His specialized interests are fault protection, detection, classification, and location in HVAC and HVDC transmission lines, control of reactive power and FACTS devices, evaluation and improvement of power quality, and power system studies.